AIAA 82-4126

A Nongyroscopic Inertial Measurement Unit

Shmuel J. Merhav*
Technion—Israel Institute of Technology, Haifa, Israel

This paper describes a concept of a low-cost gyroless inertial measurement unit. By means of an orthogonal triad of rotating or vibrating accelerometers, angular rates are measured along with specific forces. The precise separation of the two signals from the accelerometer readings is described. Apart from its simplicity, the special features of the separation method are that signal bandwidth is not sacrified, inertial angular rate measurements are essentially drift-free, and dynamical errors due to angular rate and specific force derivatives are reduced to negligible values. A detailed statistical analysis of the error sources, due to dynamical effects, sampling, nonlinearities, and vibration is given. The residual angular rate offset is due to the electronic processor which, with modern CMOS components, is shown to provide a performance level in the 1 n.mi./h class. The possibility of dispensing with the costly gyroscopes, which are essential in conventional designs, indicates a substantial saving in cost.

Nomenclature

a	= vector of accelerometer outputs
a	= bandwidth of random process
b	= index of body axes
c	= index of coherent terms
F	= vector of specific forces applied to vehicle
g	= gravity vector
$h(t)$	= impulse response
i	= index of coordinates x,y,z
l	= distance vector
m	= ratio of frequencies
n	= vector of measurement noise
o	= index of orthogonal terms
p,q,r	= components of angular rate
R_E	= radius of Earth
$\tilde{R}$	= position error
t	= time
T	= period of cycle
u	= normalized distance function
V	= vibration amplitude
X,Y,Z	= rectangular coordinate system
α	= bandwidth normalized to Schuler frequency ω_s
ζ	= normalized time $\zeta=\omega_s t$
μ	= beat frequency
ν	= vibration frequency
τ	= time difference
ρ	= radius of rotation or amplitude of vibration
σ	= standard deviation
$\phi(\cdot)$	= autocorrelation function
$\Phi(\cdot)$	= power density spectrum
$\Phi^*(\cdot)$	= power density spectrum of sampled signal
ω	= frequency of revolution
ω_s	= Schuler frequency
Ω	= angular rate vector of body axis system
$\tilde{\Omega}_i$	= component of angular rate error

I. Introduction

THROUGHOUT the past two decades, the high cost of inertial navigation systems (INS) has presented a continuing challenge in the search for low-cost mechanization and instrumentation. Alternative approaches have either involved departures from classical sensor realizations based on mechanical gyroscopes,[1-3] or novel concepts of inertial measurement unit (IMU) mechanizations.[4,5] The principal trend that has emerged from these efforts is the strapdown concept,[6] with its greatly simplified mechanization but higher demands on the gyroscopes.[7] In consequence, the challenge for substantial cost reduction still persists. In conventional designs the specific forces triad $F=[F_x,F_y,F_z]'$ and the angular rate triad $\Omega=[p,q,r]'$ are independently measured by accelerometers and gyroscopes. The major issue since the inception of INS technology has been the high cost of gyroscopes, which constitutes the principal part of the IMU cost, and is as yet in the $10,000 range per unit. Accelerometers, however, with INS quality[8] have become available in the $1000 range per unit. It is therefore highly desirable to devise an IMU without gyroscopes so that both F and Ω are measured by accelerometers only. A number of accelerometer based IMU concepts have been reported,[1,2,9] but apparently have not matured into practical technologies.

In this paper, a concept of rotating or vibrating accelerometers suitable for strapdown and gimballed realization is presented and analyzed in detail. The problem is to analyze and evaluate the various contributions to errors in F and Ω, and to determine whether the corresponding signals provided by the accelerometers can be separated with sufficient precision. Based on state-of-the-art accelerometers[8] and recent CMOS component data,[10] the analysis shows that the principal error sources, i.e., null point offsets, linearity, dynamic response, and random measurement noise are compatible with 1 n.mi./h INS requirements. Feeding the outputs of the rotating accelerometers to the electronic processor via slip rings under MIL standard requirements has been accomplished in a mechanically similar practical realization of a novel rate sensor.[11] The key feature of the described concept is that its rate null point offset is essentially determined by the null point stability of the electronic processor. Novel CMOS amplifiers indicate that a stability better than 0.01 deg/h can be accomplished. Initial estimates indicate a substantial savings in cost, in comparison with the conventional gyro based instrumentation.

II. Principle of Operation and Basic Parameters

Three accelerometers A_x, A_y, A_z, rigidly mounted on three orthogonal platforms rotating at constant angular velocities ω, are shown in Fig. 1 in positions corresponding to $t=0$. For the simple case $\Omega=$ const., their outputs a_x,a_y,a_z are the sums of F_x,F_y,F_z, and the corresponding Coriolis forces $2q\omega\rho\cos\omega t$, $2r\omega\rho\cos\omega t$, $2p\omega\rho\cos\omega t$. Since ω and ρ are known constants, q, r, p, can, in principle, be separated from F_x, F_y, F_z so that all the basic IMU information is provided by the three rotating accelerometers A_x, A_y, A_z.

Received June 22, 1981; revision received Dec. 2, 1981.

*Professor, Department of Aeronautical Engineering. Member AIAA.

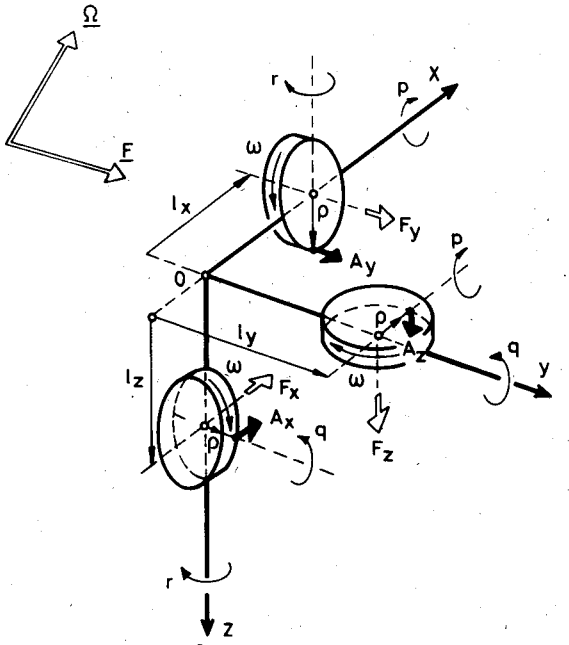

Fig. 1 Orientation of rotating accelerometers in an orthogonal body fixed axis system, shown at positions corresponding to $t=0$.

In reality, however, $a=(a_x,a_y,a_z)'$ includes, in addition, a number of interfering signals resulting from angular accelerations, angular rate cross products, bias and noise components nonlinearities, and dynamical errors. The analysis in the following sections shows that these error sources are of a negligibly low level or can be compensated.

In order to examine the feasibility of the concept, consider e.g., A_y and disregard for the moment F_y. Due to the yaw rate r, the amplitude of a_y is $a_y=2\omega\rho r$. The following assumptions are now made:

$$r_{\max}=200 \text{ deg/s}\cong 3.5 \text{ rad/s} \qquad r_{\min}=0.1 \text{ deg/h}$$

$$\omega=200 \text{ rad/s} \qquad \rho=1.5\times 10^{-2} \text{ m}$$

Thus,

$$a_{y\max}=2\times 200\times 1.5\times 10^{-2}\times 3.5=20 \text{ m/s}^2\cong 2g$$

and the required dynamic range R_r is

$$R_r=r_{\max}/r_{\min}=200\times 3600/0.1=7.2\times 10^6$$

A typical accelerometer[8] has a static threshold of $10^{-6}g$. With dither it can be effectively reduced to $\sim 10^{-7}g$ so that the actual dynamic range R_a is $R_a=2g/10^{-7}g=20\times 10^6$. Thus, R_r can be achieved with a typical accelerometer.

In the actual realization, the measured range is divided into two regions, e.g., a low range up to 20 deg/s and high range from 20 deg/s to 200 deg/s. Thus, R_r for the low range is 7.2×10^5. A typical maximum accelerometer output is $V_{\max}=10V$. Thus, the smallest significant output $V_{\min}=10/7.2\times 10^5=14\ \mu V$. The electronic processor for separating Ω from F, described later in detail, is realized by operational amplifiers, which have a null point stability of the order of 1 μV. Thus, the signal processing circuits are not expected to add a significant error to the Ω and F measurements.

III. Analysis and Signal Separation

A. Dynamics

The general equation for total acceleration measurable at a point mass moving in a rotating system is

$$a=F+\dot{\Omega}\times r+2\Omega\times\left.\frac{dr}{dt}\right|_b+\Omega\times(\Omega\times r)+\left.\frac{d^2r}{dt^2}\right|_b \qquad (1)$$

where Ω is the angular velocity vector of the system and r, the instantaneous distance of the point mass from the center of rotation of the system. In particular, with reference to Fig. 1, $r=\rho+l$ and ρ is the instantaneous vector distance of the point mass from its center of revolution and l the fixed distance of the element's center of revolution to the system center of rotation. The index b indicates differentiation with respect to the rotating body axes. Equation (1) can now be rewritten as follows:

$$a=F+\dot{\Omega}\times(\rho+l)+2\Omega\times\left.\frac{d\rho}{dt}\right|_b+\Omega\times[\Omega\times(\rho+l)]+\left.\frac{d^2\rho}{dt^2}\right|_b \qquad (2)$$

Substituting $\rho=[\rho_x\sin\omega t,\ \rho_y\sin\omega t,\ \rho_z\sin\omega t]'$, incorporating the noise components n_x, n_y, n_z respectively and resolving a into a_x, a_y, and a_z letting $\rho_x=\rho_y=\rho_z=\rho$, and rearranging terms we have

$$a_x=F_x+l_z(\dot{q}+pr)+2\omega\rho\cos\omega t\left(q-\frac{\dot{r}}{2\omega}\right)+2\omega\rho\sin\omega t\left(r+\frac{\dot{q}}{2\omega}\right)+p\rho(q\cos\omega t+r\sin\omega t)+n_x \qquad (3)$$

$$a_y=F_y+l_x(\dot{r}+qp)+2\omega\rho\cos\omega t\left(r-\frac{\dot{p}}{2\omega}\right)+2\omega\rho\sin\omega t\left(p+\frac{\dot{r}}{2\omega}\right)+q\rho(r\cos\omega t+p\sin\omega t)+n_y \qquad (4)$$

$$a_z=F_z+l_y(\dot{p}+rq)+2\omega\rho\cos\omega t\left(p-\frac{\dot{q}}{2\omega}\right)+2\omega\rho\sin\omega t\left(q+\frac{\dot{p}}{2\omega}\right)+r\rho(p\cos\omega t+q\sin\omega t)+n_z \qquad (5)$$

Each of the noise signals $n=[n_x,n_y,n_z]'$ is assumed to consist of three components as follows:

$$n=n_d+n_v+n_r$$

where n_d is low-frequency (drift) noise, n_v is sinusoidal (vibration) noise, and n_r is random zero-mean high-frequency noise.

B. Principle of Signal Separation

Denoting the computed values of p,q,r by $\hat{p},\hat{q},\hat{r}$, respectively, they can be determined from Eqs. (3-5) as follows:

$$\hat{p}=\frac{1}{8\rho}\int_0^T a_z\,\text{sgn}\cos\omega t\,dt \qquad (6)$$

$$\hat{q}=\frac{1}{8\rho}\int_0^T a_x\,\text{sgn}\cos\omega t\,dt \qquad (7)$$

$$\hat{r}=\frac{1}{8\rho}\int_0^T a_y\,\text{sgn}\cos\omega t\,dt \qquad (8)$$

or, alternatively, $\hat{q},\hat{r},\hat{p}$, by using the modulation function $\text{sgn}(\sin\omega t)$. The factor $1/8\rho$ is required for proper scaling as shown below. $T=2\pi/\omega$ is the period of a complete revolution. The choice of the sgn modulation function is due to its simplicity of realization as shown later.

To demonstrate the principle of signal separation, assume first $n_v=0$, $n_r=0$, $n_d=\text{const.}$ and that p,q,r, F_x,F_y,F_z are constant throughout T. The foregoing is illustrated in Fig. 3.

Substituting Eqs. (3-5) with all the time derivatives zero into Eqs. (6-8), respectively, only the coherent terms with $\text{sgn}(\cos\omega t)$ are retained, thus:

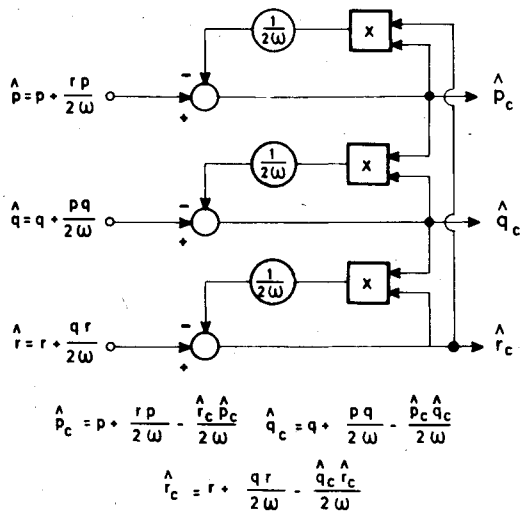

Fig. 2 Compensation of errors in angular rates due to dynamical coupling.

$$\hat{p}=\frac{1}{8\rho}(2\omega\rho p+\rho rp)\int_0^T \cos\omega t\,\mathrm{sgn}\,\cos\omega t\,dt$$

$$=\frac{2\omega p+rp}{8\omega}\int_0^{2\pi}\cos\omega t\,\mathrm{sgn}\,\cos\omega t\,d(\omega t)$$

$$=\frac{(2\omega+r)p}{2\omega}\int_0^{\pi/2}\cos\omega t\,\mathrm{d}(\omega t)=p+\frac{rp}{2\omega} \tag{9}$$

Thus, for p,q,r we have

$$\hat{p}=p(1+r/2\omega)\qquad \hat{q}=q(1+p/2\omega)\qquad \hat{r}=r(1+q/2\omega) \tag{10}$$

Thus, even with $\Omega=$ const., dynamic scale factor errors $r/2\omega$, $p/2\omega$, $q/2\omega$, respectively, may be present due to cross-products of angular rates. These, however, can be compensated as indicated in Fig. 2, in which $\hat{p}_c,\hat{q}_c,\hat{r}_c$ denote compensated computed angular rates.

The relations indicated in Fig. 2 can be written as

$$\begin{aligned}\hat{p}_c(1+\hat{r}_c/2\omega)&=p(1+r/2\omega)\\ \hat{q}_c(1+\hat{p}_c/2\omega)&=q(1+p/2\omega)\\ \hat{r}_c(1+\hat{q}_c/2\omega)&=r(1+q/2\omega)\end{aligned} \tag{11}$$

from which it follows that the compensation scheme in Fig. 2 enforces the solutions $\hat{p}_c=p$; $\hat{q}_c=q$; $\hat{r}_c=r$ as required. Possible offset errors in the multipliers are readily shown to have a negligibly small effect.

The specific forces F_x, F_y, F_z are determined by

$$\begin{aligned}\hat{F}_x&=\frac{1}{T}\int_0^T a_x\mathrm{d}t=F_x+l_z pr+n_{dx}\\ \hat{F}_y&=\frac{1}{T}\int_0^T a_y\mathrm{d}t=F_y+l_x qp+n_{dy}\\ \hat{F}_z&=\frac{1}{T}\int_0^T a_z\mathrm{d}t=F_z+l_y rq+n_{dz}\end{aligned} \tag{12}$$

The angular rate cross-product terms in Eq. (12) can easily be compensated by means of $\hat{p},\hat{q},\hat{r}$.

All the periodic terms in Eqs. (3-5) drop on integrating over the period T.

Comments

1) In principle, the measurement unit acts as a two-axis rate gyro since two components of Ω can be determined from each rotating accelerometer. In the analysis, however, each measurement unit is treated as single axis.

2) Due to the synchronous signal processing, bias terms are eliminated, and the measurement unit is essentially a drift-free rate sensor.

3) The concept can alternatively be realized by vibrating accelerometers. The advantage is the saving of slip rings and the avoidance of errors due to orthogonal components of Ω_i [Eqs. (3-5)]. A possible disadvantage is alternating forces, which may cause unwanted vibrations.

4) Simple integration of a_i over T yields the required triad of specific forces. Errors in determining F_i are the same as in conventional mechanizations.

C. Outline and Method of Error Analysis

In Secs. IV-IX a detailed analysis of the effect of errors $\tilde{\Omega}_i$ in Ω_i and $\tilde{F}_i$ in F_i on positional divergence is given. The principal error sources investigated are:

1) Dynamical errors: Within the period of integration, the accelerometer signals a_i $(i=x,y,z)$ vary due to random variations in Ω_i and F_i. These variations result in dynamical errors in $\hat{\Omega}_i$ and $\hat{F}_i$ denoted by $\tilde{\Omega}_i\triangleq\hat{\Omega}_i-\Omega_i$ and $\tilde{F}_i\triangleq\hat{F}_i-F_i$. Each of these is further specialized, e.g., $\tilde{\Omega}_{F_i}$ or $\tilde{F}_{\Omega_i}$ where the subscript denotes the origin of the error. Each term in Eqs. (3-5) except those multiplying $2\rho\omega\cos\omega t$ is considered a source of a dynamical error and is analyzed separately.

2) Error due to sampling: The continuous formulation of the dynamical errors shows that the power density spectra have zeros at zero frequency. This would result in greatly reduced positional divergence. However, since the signals are sampled, the power density spectrum is not zero. These error sources denoted by $\tilde{\Omega}_i^*$ and $\tilde{F}_i^*$ greatly contribute to positional divergence.

3) Errors due to periodic vibration: These errors, denoted by $\tilde{\Omega}_{iv}$ and $\tilde{F}_{iv}$ are analyzed as a function of the ratio $\nu/\omega=m$ where ν is the vibration frequency.

4) Errors due to wide band random accelerometer noise: A noise model based on a typical forced balance accelerometer, after the processing of the signal separator is greatly reduced and is denoted by $\tilde{\Omega}_{ni}$ and $\tilde{F}_{ni}$.

5) Accelerometer nonlinearities: Both even and odd nonlinearities are considered. It is shown that their effects are random scale factor errors.

6) Misalignment and cross-axis errors: Due to centripetal force, these errors are essentially dc and are eliminated in the Ω_i measurement. They are less critical in the F_i measurement, and can be compensated. This error source is therefore not addressed.

It is assumed that F_i and Ω_i, resulting from control or turbulence, are described by Markov processes with bandwidths $a\gg\omega_s$. As a result, all the dynamical error models can practically be modeled as zero mean white noise processes so that computation of positional divergence is greatly simplified. Similar assumptions are made for the other error sources. Every error source, $\tilde{\Omega}_i$ and $\tilde{F}_i$ described below in detail, is given by its power density spectrum or autocorrelation function. Let $\Phi_{\tilde{\Omega}_i}(s)$ and $\Phi_{\tilde{F}_i}(s)$ denote the power spectra of $\tilde{\Omega}_i$ and $\tilde{F}_i$, respectively. The corresponding power spectra of positional divergence $\Phi_{\tilde{R}\tilde{\Omega}_i}(s)$ and $\Phi_{\tilde{R}\tilde{F}_i}(s)$ are

$$\Phi_{\tilde{R}\tilde{\Omega}_i}(s)=\frac{\Phi_{\tilde{\Omega}_i}(s)g^2}{(-s^2)(\omega_s^2+s^2)[\omega_s^2+(-s^2)]} \tag{13}$$

$$\Phi_{\tilde{R}\tilde{F}_i}(s)=\frac{\Phi_{\tilde{F}_i}(s)}{(\omega_s^2+s^2)[\omega_s^2+(-s^2)]} \tag{14}$$

which represent the Schuler pendulum response to the random input noise spectrum.

Because of the imaginary pole pairs $\pm j\omega_s$, where $\omega_s=$ Schuler frequency, the frequency domain integrals of Eqs. (13) and (14) do not converge, and the integrations must be performed in time domain. Since white noise models have

been assumed, these integrals take the form

$$\sigma^2_{\tilde{R}\tilde{\Omega}_i}(t) = \int_0^t [h_{\tilde{R}\tilde{\Omega}_i}(\tau)]^2 d\tau \tag{15}$$

$$\sigma^2_{\tilde{R}\tilde{F}_i}(t) = \int_0^t [h_{\tilde{R}\tilde{F}_i}(\tau)]^2 d\tau \tag{16}$$

where

$$h_{\tilde{R}\tilde{\Omega}_i}(t) = \mathcal{L}^{-1}\left[\Phi^+_{\tilde{R}\tilde{\Omega}_i}(s)/s(\omega_s^2+s^2)\right]$$

and

$$h_{\tilde{R}\tilde{F}_i}(t) = \mathcal{L}^{-1}\left[\Phi^+_{\tilde{R}\tilde{F}_i}(s)/(\omega_s^2+s^2)\right]$$

$\Phi^+_{\tilde{R}\Omega_i}(s)$ and $\Phi^+_{\tilde{R}F_i}(s)$ are the left-plane factors of the corresponding power spectra and $\sigma^2_{\tilde{R}\tilde{\Omega}_i}(t)$, $\sigma^2_{\tilde{R}\tilde{F}_i}(t)$ are the positional divergence variances.

The general form of Eqs. (15) and (16), on taking square roots for $\sigma_{\tilde{R}}(t)$, is

$$\sigma_{\tilde{R}}(\zeta) = Ku(\zeta,\alpha) \tag{17}$$

where K is a constant involving the radius of the Earth, R_E, ω_s, and input parameters; u is dimensionless range; $\zeta \triangleq \omega_s t$ and $\alpha \triangleq a/\omega_s$. For each particular $\tilde{\Omega}_i$ or $\tilde{F}_i$ the appropriate K and $u(\zeta,\alpha)$ will be explicitly given so that the appropriate value of $\sigma_{\tilde{R}}(\zeta)$ can be determined for each error source. Because of the additional integration, errors due to $\tilde{\Omega}_i$ are more significant than those due to $\tilde{F}_i$.

IV. Dynamical Errors in Angular Rates

In this section, a detailed analysis of error sources in $\hat{\Omega}$ is presented. In particular, it is shown that the effect of the signal processor is such that only small residual errors proportional to the first or second derivative of F or Ω exist. Consequently, the power spectra of these errors have single or double zero at zero frequency. Thus, the resulting positional divergence is considerably reduced and is represented by expressions that differ from standard first order Markov models.

A. Time Derivatives of Forces

$F = F(t) = [F_x(t), F_y(t), F_z(t)]'$ varies throughout T, and is developed into a Taylor series with respect to $t=0$ in the interval $(0,T)$.

$$F(t) = F + \dot{F}t + \ddot{F}t + \dddot{F}(t^2/2) + \ldots + 0(t^3) \quad (0<t<T) \tag{18}$$

Recalling the operation $F_i \mathrm{sgn}(\cos\omega t)$ and Fig. 3, the integrals in Eqs. (6-8) yield a residual error in $\hat{\Omega}$ denoted by

$$\tilde{\Omega}_F = [\tilde{\Omega}_{F_x} \triangleq \tilde{q}_F, \quad \tilde{\Omega}_{F_y} \triangleq \tilde{r}_F, \quad \tilde{\Omega}_{F_z} \triangleq \tilde{p}_F]'$$

Denoting any component of $\tilde{\Omega}_F$ by $\tilde{\Omega}_{F_i}$ $(i=x,y,z)$ we have:

$$\tilde{\Omega}_{F_i} = \frac{1}{8\rho}\left\{\int_0^{T/4} F_i(t)\,dt - \int_{T/4}^{3T/4} F_i(t)\,dt + \int_{3T/4}^{T} F_i(t)\,dt\right\} \tag{19}$$

Substituting Eq. (18) into Eq. (19), the result is

$$\tilde{\Omega}_{F_i} = \ddot{F}_i(T^3/256\rho) = \ddot{F}_i(\pi^3/32\rho\omega^3) \tag{20}$$

Substituting the numerical values $\rho = 1.5\times10^{-2}$ m and $\omega = 200$ rad/s, then $\tilde{\Omega}_{F_i} = = 8\times10^{-6}\ddot{F}_i$ rad/s.

In order to ensure a physically valid statistical model for $\tilde{\Omega}_{F_i}$ we model F_i by an everywhere twice differentiable autocorrelation function resulting from an isotropic random stationary atmospheric turbulence model

$$\phi_{F_i}(\tau) = \sigma^2_{F_i}(1 + a|\tau| + \tfrac{1}{3}a^2|\tau|^2)e^{-a|\tau|} \tag{21}$$

The corresponding power spectrum is $\sigma^2_{F_i}(16/3)a^5/(a^2-s^2)^3$ and with Eq. (20)

$$\Phi_{\tilde{\Omega}_{F_i}}(s) = \sigma^2_{F_i}\left(\frac{\pi^3}{32\rho\omega^3}\right)^2 \frac{16}{3}\frac{a^5 s^4}{(a^2-s^2)^3} \tag{22}$$

The resulting spectrum of positional divergence is

$$\Phi_{\tilde{R}\tilde{\Omega}_{F_i}}(s)$$

$$= \sigma^2_{F_i}\left(\frac{\pi^3}{32\rho\omega^3}\right)^2 \frac{16}{3} g^2 \frac{a^5}{(a^2-s^2)^3}\frac{-s^2}{(\omega_s^2+s^2)(\omega_s^2+(-s)^2)}$$

$$\approx \sigma^2_{F_i}\left(\frac{\pi^3}{32\rho\omega^3}\right)^2 \frac{16}{3}\frac{g^2}{a}\frac{-s^2}{(\omega_s^2+s^2)[\omega_s^2+(-s)^2]} \tag{23}$$

In accordance with Eq. (15)

$$h_{\tilde{R}\tilde{\Omega}_i}(t) = \mathcal{L}^{-1}[s/(\omega_s^2+s^2)] = \cos\omega_s t$$

so that $\sigma_{\tilde{R}\tilde{\Omega}_{F_i}}$ is

$$\sigma_{\tilde{R}\tilde{\Omega}_{F_i}}(\zeta) = Ku(\zeta,\alpha) = 1.58\frac{\sigma_{F_i}}{\omega^2}\frac{R_E\omega_s}{\rho\omega}\left[\frac{1}{\alpha}\left(\zeta + \frac{\sin 2\zeta}{2}\right)\right]^{1/2} m \tag{24}$$

With the asumed numerical values for ω,ρ, and with $a=1$ rad/s and $\sigma_{F_i} = 1$ m/s^2 we have

$$\sigma_{\tilde{R}\tilde{\Omega}_{F_i}}(\zeta) = 2.3\times10^{-3}\left[\zeta + \frac{\sin 2\zeta}{2}\right]^{1/2} m \tag{25}$$

which is a negligibly small error.

B. Time Derivatives of Angular Rates

Developing $\Omega_i(t)$ into a Taylor series in $(0,T)$.

$$\Omega_i(t) = \Omega_i + \dot{\Omega}_i t + \ddot{\Omega}_i(t^2/2) + \cdots + 0(t^3) \tag{26}$$

and recalling Eqs. (3-8), $\hat{\Omega}_i$ resulting from the coherent components $\Omega_i^c \triangleq \Omega_i(t)\cos\omega t\,\mathrm{sgn}(\cos\omega t)$ will be denoted by $\hat{\Omega}_i^c$ and is given by

$$\hat{\Omega}_i^c = \frac{1}{8\rho}2\omega\rho\int_0^T \Omega_i(t)\cos\omega t\,\mathrm{sgn}(\cos\omega t)\,dt$$

$$= \frac{1}{4}\left[\int_0^{2\pi}\Omega_i(t)\cos\omega t\,d(\omega t) - \int_{\pi/2}^{3\pi/2}\Omega_i(t)\cos\omega t\,d(\omega t) + \int_{3\pi/2}^{2\pi}\Omega_i(t)\cos\omega t\,d(\omega t)\right] \tag{27}$$

Substituting Eq. (26) into Eq. (27), the result is

$$\hat{\Omega}_i^c = \Omega_i + \dot{\Omega}_i\frac{T}{2} + \ddot{\Omega}_i\frac{T^2}{8} + \frac{\pi^2+4\pi-8}{32\pi^2}\dddot{\Omega}_i T^2 \tag{28}$$

The first three terms are the exact values of Ω_i at $t=T/2$ and the fourth term is the dynamical error, $\tilde{\Omega}_i^c$,

$$\tilde{\Omega}_i^c = \frac{\pi^2+4\pi-8}{8\omega^2}\dddot{\Omega}_i = \frac{1.8}{\omega^2}\dddot{\Omega}_i \text{ rad/s} \tag{29}$$

Assuming that $\Omega_i(t)$ is a bounded stationary process, we again assume an autocorrelation function of the same form as Eq. (21) yielding the power spectrum $\sigma^2_{\dot{\Omega}_i}(16/3)a^5/(a^2-s^2)^3$.

With Eq. (29), the power spectrum of $\tilde{\Omega}_i^c$ is

$$\Phi_{\tilde{\Omega}_i^c}(s)=\sigma_{\Omega_i}^2\left(\frac{1.8}{\omega^2}\right)^2\frac{16}{3}\frac{a^5s^4}{(a^2-s^2)^3}$$

$$\approx\sigma_{\Omega_i}^2\left(\frac{1.8}{\omega^2}\right)^2\frac{16}{3}\frac{s^4}{a}=\sigma_{\Omega_i}^2\frac{17.3}{\omega^4}\frac{s^4}{a} \tag{30}$$

The resulting spectrum of positional divergence, as in Eq. (23), is

$$\Phi_{\tilde{R}\tilde{\Omega}_i^c}\ \Phi_{\tilde{R}\tilde{\Omega}_i^c}(s)=\sigma_{\Omega_i}^2\frac{17.3}{\omega^4}\frac{g^2}{a}\frac{-s^2}{(\omega_s^2+s^2)\,[\omega_s^2+(-s)^2]} \tag{31}$$

and the positional divergence $\sigma_{\tilde{R}\tilde{\Omega}_i^c}$ is

$$\sigma_{\tilde{R}\tilde{\Omega}_i^c}(\zeta)=4.15\frac{\sigma_{\Omega_i}}{\omega}R_E\frac{\omega_s}{\omega}\left[\frac{1}{\alpha}\left(\zeta+\frac{\sin2\zeta}{2}\right)\right]^{1/2}m \tag{32}$$

Assuming $\sigma_{\Omega_i}=0.1$ rad/s, the result is

$$\sigma_{\tilde{R}\tilde{\Omega}_i^c}(\zeta)=2.88\times10^{-3}(\zeta+\sin2\zeta/2)^{1/2}m \tag{33}$$

which is a negligibly small error.

The orthogonal terms in Eqs. (3-5), denoted here by $\tilde{\Omega}_i^o$ derive from

$$\tilde{\Omega}_i^o=\frac{1}{8\rho}2\omega\rho\int_0^T\Omega_i(t)\sin\omega t\ \mathrm{sgn}(\cos\omega t)\,\mathrm{d}t$$

$$=\frac{1}{4}\left[\int_0^{2\pi}\Omega_i(t)\sin\omega t\,\mathrm{d}(\omega t)-\int_{\pi/2}^{3\pi/2}\Omega_i(t)\sin\omega t\,\mathrm{d}(\omega t)\right.$$

$$\left.+\int_{3\pi/2}^{2\pi}\Omega_i(t)\sin\omega t\,\mathrm{d}(\omega t)\right] \tag{34}$$

Substituting Eq. (26), the result is

$$\tilde{\Omega}_i^o\doteq\frac{1}{\omega}\left(1-\frac{\pi}{2}\right)\dot{\Omega}_i+\frac{\pi}{\omega^2}\left(1-\frac{\pi}{2}\right)\ddot{\Omega}_i\approx\frac{1}{\omega}\left(1-\frac{\pi}{2}\right)\dot{\Omega}_i=\frac{0.57}{\omega}\dot{\Omega}_i \tag{35}$$

Again, using the same spectrum for Ω_i as in Eq. (30), we have

$$\Phi_{\tilde{\Omega}_i^o}(s)=\sigma_{\Omega_i}^2\left(\frac{0.57}{\omega}\right)^2\frac{16}{3}\frac{a^5s^2}{(a^2-s^2)^3}\approx\sigma_{\Omega_i}^2\left(\frac{0.57}{\omega}\right)^2\frac{16}{3}\frac{s^2}{a} \tag{36}$$

The corresponding power spectrum of positional divergence is

$$\Phi_{\tilde{R}\tilde{\Omega}_i^o}(s)=\sigma_{\Omega_i}^2\frac{1.73}{\omega^2}\frac{g^2}{a\omega_s^2}\frac{\omega_s^2}{(\omega_s^2+s^2)\,[\omega_s^2+(-s)^2]} \tag{37}$$

In accordance with Eq. (15), $h_{\tilde{R}\tilde{\Omega}^o}(t)=\mathcal{L}^{-1}[\omega_s^2/(\omega_s^2+s^2)]=\sin\omega_s t$ and the resulting positional divergence is

$$\sigma_{\tilde{R}\tilde{\Omega}_i^o}(\zeta)=0.93\frac{\sigma_{\Omega_i}}{\omega}R_E\left[\frac{1}{\alpha}\left(\zeta-\frac{\sin2\zeta}{2}\right)\right]^{1/2}m \tag{38}$$

For the same numerical values as before

$$\sigma_{\tilde{R}\tilde{\Omega}_i^o}(\zeta)=103\,[\zeta-\sin2\zeta/2]^{1/2}m \tag{39}$$

This positional divergence is still quite small even after several hours of flight. Moreover, since the estimates $\hat{\Omega}_i$ of Ω_i are obtained from Eqs. (6-8), $\dot{\Omega}_i$ can be estimated, and with Eq. (35), $\hat{\tilde{\Omega}}_i^o=(0.57/\omega)\hat{\Omega}_i$ can be computed and almost completely compensated.

V. Dynamical Errors in Specific Forces

Since positional divergence due to errors $\tilde{F}_i$ involves one less integration than those due to $\tilde{\Omega}_i$, [see Eqs. (13) and (14)], their effect is by far less significant.

A. Time Derivatives of Forces

From Eqs. (12) and (18)

$$\hat{F}_{F_i}=\frac{1}{T}\int_0^T\left(F_i+\dot{F}_i t+\ddot{F}_i\frac{t^2}{2}\right)\mathrm{d}t=F_i+\dot{F}_i\frac{T}{2}+\ddot{F}_i\frac{1}{2}\left(\frac{T}{2}\right)^2 \tag{40}$$

which is the exact value of F_i at $T/2$, and no error is introduced beyond the sampling error.

B. Time Derivatives of Angular Rates

The coherent terms contribute the error:

$$\tilde{F}_{\Omega_i^c}=\frac{1}{T}\int_0^T2\omega\rho\Omega_i(t)\cos\omega t\,\mathrm{d}t$$

$$=\frac{1}{2\pi}2\omega\rho\int_0^{2\pi}\left(\Omega_i+\frac{\dot{\Omega}_i}{\omega}\omega t+\frac{\ddot{\Omega}_i}{\omega^2}\frac{(\omega t)^2}{2}\right)\cos\omega t\,\mathrm{d}(\omega t)=\frac{2\rho}{\omega}\ddot{\Omega}_i \tag{41}$$

This is of the same form as Eq. (29), but being an acceleration error its effect on positional divergence is even less significant. Similary, the orthogonal terms cause the error $\tilde{F}_{\Omega_i^o}$ given by

$$\tilde{F}_{\Omega_i^o}=\frac{1}{2\pi}2\omega\rho\int_0^{2\pi}\left(\Omega_i+\frac{\dot{\Omega}_i}{\omega}\omega t+\frac{\ddot{\Omega}_i}{\omega^2}\frac{(\omega t)^2}{2}\right)\sin\omega t\,\mathrm{d}(\omega t)\cong-2\rho\dot{\Omega}_i \tag{42}$$

This is of the same form as Eq. (35), but being an acceleration error and, moreover, since a good estimate $\hat{\dot{\Omega}}_i$ is available $\tilde{F}_{\Omega_i^o}$ can almost completely be compensated.

C. Errors Due to Tangential Accelerations and Angular Rate Cross-Products

The component $\dot{\Omega}\times l$ as given in Eq. (2) is of the same nature as F, and can therefore be treated as one of its components. Since l is normally of the order of 1 m or less, and $\sigma_{\dot{\Omega}_i}$ is assumed to be in the order of 0.1 rad/s, with a ≈1 rad/s, $\sigma_{\dot{\Omega}_i}=a\sigma_{\Omega_i}$ 0.1 rad/s^2, and $l\sigma_{\dot{\Omega}_i}\neq0.1$ m/s^2. Also with the spectrum assumed for Ω, this acceleration component has an additional zero at the origin $s=0$, and is less significant than other terms in F_i. Errors due to $l_z pr$, $l_x qp$, and $l_y rq$ in Eqs. (3-5) are of the same nature as $\tilde{F}_i$, and are negligibly small. Errors due to the terms $\dot{r}/2\omega$, $\dot{q}/2\omega$, and $\dot{p}/2\omega$ are clearly negligible.

VI. Errors Due to Sampling

A. Power Density Spectrum at Zero Frequency

As indicated in Fig. 3, $\hat{F}_i$ and $\hat{\Omega}_i$ are obtained in sampled format at a frequency $f=2\pi/T$. Thus, the actual signals, not being continuous, will not have zeros in the power spectra of $\ddot{\Omega}_i$ or $\dot{\Omega}_i$ as indicated, e.g., in Eq. (22) or Eq. (36). Consequently, there exists some power density at zero frequency, and the actual positional divergence is not exactly in accordance with the foregoing analysis. The additional positional divergence due to sampling is analyzed below. Assuming an autocorrelation function for Ω_i as in Eq. (21),

$$\phi_{\Omega_i}(\tau)=\sigma_{\Omega_i}^2(1+a|\tau|+\tfrac{1}{3}a^2|\tau|^2)e^{-a|\tau|} \tag{43}$$

Correspondingly, $\phi_{\dot{\Omega}_i}(\tau)$ is

$$\phi_{\dot{\Omega}_i}(\tau)=\frac{\mathrm{d}^4\phi_{\Omega_i}(\tau)}{\mathrm{d}\tau^4}=\sigma_{\dot{\Omega}_i}^2a^4\left(1-\frac{5}{3}a|\tau|+\frac{1}{3}a^2|\tau|^2\right)e^{-a|\tau|} \tag{44}$$

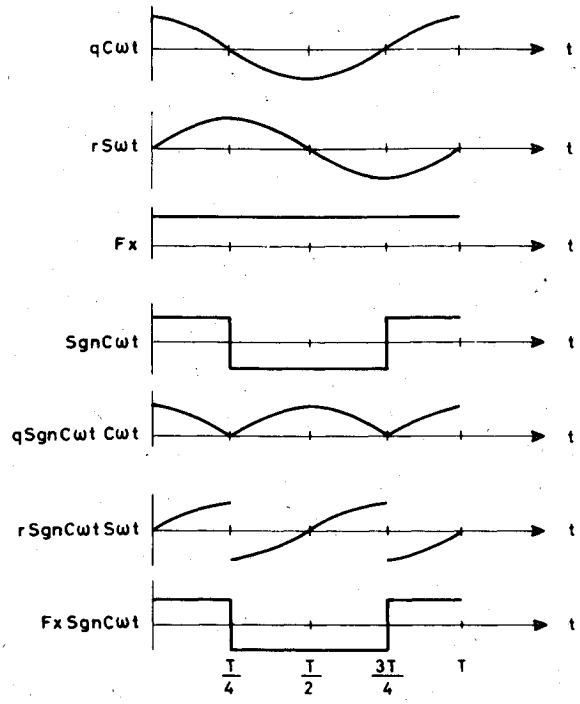

Fig. 3 Accelerometer output signal processing.

It is easily verified that the power spectrum at zero frequency $\Phi_{\tilde{\Omega}_i}(0)$ is

$$\Phi_{\tilde{\Omega}_i}(0) = 2\int_0^\infty \phi_{\tilde{\Omega}_i}(\tau)\,d\tau = 0 \tag{45}$$

The autocorrelation function of a sampled process is given by

$$\phi^*_{\tilde{\Omega}_i}(\tau) = \phi_{\Omega_i}(nT) + (\phi_{\Omega_i}[(n+1)T] - \phi_{\Omega_i}(nT))\tau/T \qquad (n=1,2,\ldots) \tag{46}$$

Substituting Eq. (44) into Eq. (46), and replacing the integral (45) by an infinite sum, we obtain the sampled power spectrum at zero frequency:

$$\Phi^*_{\tilde{\Omega}_i}(0) = 2\sigma^2_{\tilde{\Omega}_i} a^4 T\left[T + \left(\sum_{n=1}^{\infty} e^{-anT} - \sum_{n=1}^{\infty} \frac{5}{3} anTe^{-anT} + \sum_{n=1}^{\infty} \frac{1}{3} a^2 n^2 T^2 e^{-anT}\right)\right] \tag{47}$$

The sums in Eq. (47) are geometric series and their respective derivatives, thus, they can be expressed in closed form as follows:

$$\Phi^*_{\tilde{\Omega}_i}(0) = \frac{2\sigma^2_{\tilde{\Omega}_i} a^4}{a}\left\{aT\left[\frac{1}{2} + \frac{e^{-aT}}{1-e^{-aT}} - \frac{5}{3}\frac{aTe^{-aT}}{(1-e^{-aT})^2} + \frac{1}{3}\frac{a^2T^2e^{-aT}(1+e^{-aT})}{(1-e^{-aT})^3}\right]\right\} \tag{48}$$

Denoting the expression in parentheses by $H(aT)$ and since $\sigma^2_{\tilde{\Omega}_i} a^4 = \sigma^2_{\dot{\tilde{\Omega}}_i}$, Eq. (48) can be rewritten as

$$\Phi^*_{\tilde{\Omega}_i}(0) = (2\sigma^2_{\dot{\tilde{\Omega}}_i}/a) H(aT) \tag{49}$$

B. Coherent Components of Angular Rates

The corresponding angular rate error spectrum is obtained by scaling Eq. (49) by Eq. (29)

$$\Phi^{*c}_{\tilde{\Omega}_i}(0) = 2(1.8/\omega^2)^2(\sigma^2_{\dot{\tilde{\Omega}}_i}/a) H(aT) \tag{50}$$

and the angular rate error variance is

$$\sigma^{*c}_{\tilde{\Omega}_i} = 2(1.8/\omega^2)^2(\sigma^2_{\dot{\tilde{\Omega}}_i} H(aT) \tag{51}$$

with the same numerical values for T, a, ω, and σ_{Ω_i} as before we have $H(aT) = 2\times10^{-4}$ and $\sigma^{*c}_{\tilde{\Omega}_i} = 9\times10^{-8}$ rad/s.

The corresponding impulse response

$$h_{\tilde{R}}(t) = \mathcal{L}^{-1}[1/s(\omega_s^2+s^2)] = (1-\cos\omega_s t)/\omega_s^2 \tag{52}$$

and the resulting positional divergence is

$$\sigma^*_{\tilde{R}\tilde{\Omega}^c_i}(\zeta) = \frac{\sigma^{*c}_{\tilde{\Omega}_i} R_E}{\omega_s}\left[\frac{1}{\alpha}\left(3\zeta - 4\sin\zeta + \frac{\sin 2\zeta}{2}\right)\right]^{1/2} \tag{53}$$

at $t=1$ h corresponding to $\zeta = 4.46$ rad/s, the result is $\sigma^*_{\tilde{R}\tilde{\Omega}^c_i} = 65$ m.

In a similar way, the error $\sigma^*_{\tilde{R}_{F_i}}$ due to the sampling of F_i can be determined. Again, since divergence due to $\tilde{F}_i$ is much less significant, it is not discussed in further detail.

C. Orthogonal Components of Angular Rates

In a similar manner the error due to the orthogonal terms, Eq. (35), can be analyzed:

$$\phi_{\dot{\Omega}_i}(\tau) = -\frac{d^2\phi_{\Omega_i}(\tau)}{d\tau^2} = \sigma^2_{\dot{\Omega}_i}\frac{a^2}{3}[1+a|\tau| - a^2|\tau|^2]e^{-a|\tau|} \tag{54}$$

Again, using Eq. (46), and computing the corresponding infinite sum to obtain $\Phi^*_{\dot{\tilde{\Omega}}_i}(0)$, we have

$$\Phi^*_{\dot{\tilde{\Omega}}_i}(0) = (2/a)\sigma^2_{\dot{\Omega}_i}(a^2/3)G(aT) = (2/a)\sigma^2_{\dot{\Omega}_i} G(aT) \tag{55}$$

where

$$G(aT) \triangleq aT\left[\frac{1}{2} + \frac{e^{-aT}}{1-e^{-aT}} + \frac{aTe^{-aT}}{(1-e^{-aT})^2} - \frac{a^2T^2e^{-aT}(1+e^{-aT})}{(1-e^{-aT})^3}\right] \tag{56}$$

with the same numerical values as before, $G(aT) = 8\times10^{-9}$. From Eq. (35), the corresponding value $\Phi^{*\rho}_{\dot{\tilde{\Omega}}_i}(0)$ is $(0.57/\omega)^2$ $\Phi^*_{\dot{\tilde{\Omega}}_i}(0)$ and $\sigma^{*\rho}_{\dot{\tilde{\Omega}}_i}$ is

$$\sigma^{*\rho}_{\dot{\tilde{\Omega}}_i} = \sqrt{2/3}\,(0.57/\omega)\sigma_{\dot{\Omega}_i} a\sqrt{G(aT)} = 2.2\times10^{-8}\ \text{rad/s} \tag{57}$$

The resulting positional divergence is of the same form as Eq. (53), and it would yield at 1 h, $\zeta = 4.46$ rad, the divergence $\sigma^*_{\tilde{R}\tilde{\Omega}^\rho_i} = 16$ m.

VII. Effects of Periodic Vibration

A periodic vibration noise vector $n_v \triangleq (n_{v_x}, n_{v_y}, n_{v_z})'$ is defined by its components

$$n_{v_i} = V_i\cos(\nu t + \phi) \tag{58}$$

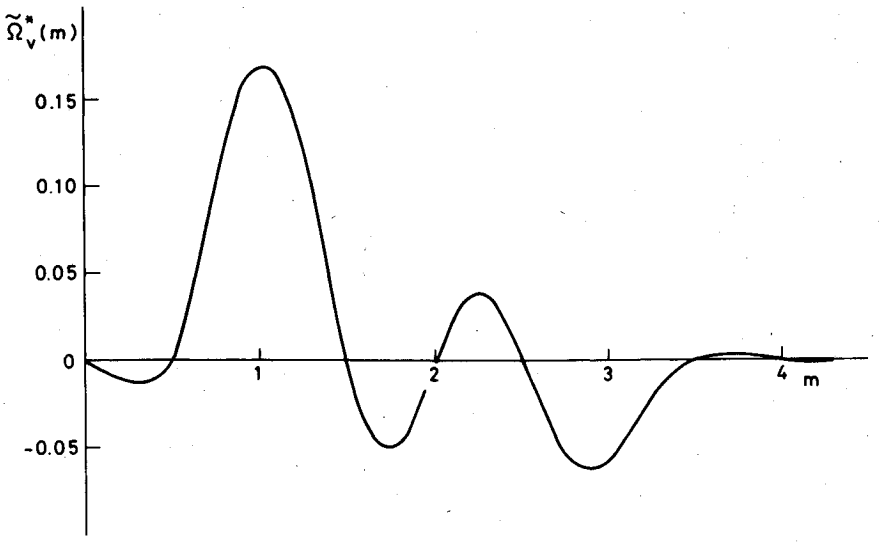

Fig. 4 Amplitude of vibration error $\tilde{\Omega}^*_v$ as a function of relative vibration frequency $m=\nu/\omega$.

where V_i, $(i=x,y,z)$ is the amplitude of the vibration acceleration, and ϕ is a random constant phase angle. The resulting noise in $\hat{\Omega}_i$ is

$$\tilde{\Omega}_{v_i} = \frac{V_i}{8\rho}\int_0^T \cos(\nu t+\phi)\,\mathrm{sgn}(\cos\omega t)\,dt$$

$$= \frac{V_i}{2\rho\nu}\sin\frac{\nu T}{4}\left(\cos\frac{\nu T}{4}-1\right)\cos\left(\frac{\nu T}{2}+\phi\right) \tag{59}$$

Substituting $T\triangleq 2\pi/\omega$, $\nu/\omega\triangleq m$,

$$\tilde{\Omega}^*_{v_i} = \frac{V_i}{2\rho m\omega}\sin\frac{m\pi}{2}\cos(m\pi+\phi)\left(\cos\frac{m\pi}{2}-1\right) \tag{60}$$

with $\nu=$ const. and $\phi(0)=\phi_0$, the phase angle with respect to the reference frequency ω is

$$\phi(t)=\phi_0+(\nu-\omega)t \tag{61}$$

Since the output is sampled at intervals T,

$$\phi^*(nT)=\phi_0+(\nu-\omega)nT=\phi_0+(m-1)2\pi n \qquad (n=1,2,3,\ldots) \tag{62}$$

Substituting Eq. (62) into Eq. (60), and letting $\phi_0=0$

$$\tilde{\Omega}^*_{v_i} = \frac{V_i}{2\rho m\omega}\sin\frac{m\pi}{2}\left(\cos\frac{m\pi}{2}-1\right)\cos(\pi m+2(m-1)\pi n) \tag{63}$$

For a given value of m, $\tilde{\Omega}^*_{v_i}$ is periodic in n, the amplitude decreasing with m. For example, for $n=0$ and with, e.g., $V_i=1$ m/s^2, $\omega=200$ rad/s, $\rho=1.5\times10^{-2}$ m,

$$\tilde{\Omega}^*_{v_i} = \frac{1}{6m}\sin\frac{m\pi}{2}\left(\cos\frac{m\pi}{2}-1\right) \tag{64}$$

A plot of Eq. (64) is shown in Fig. 4. From it, it follows that $\tilde{\Omega}^*_{v_i}(m)$ becomes very small for $m>3.5$, corresponding to $\nu=700$ or ~ 100 Hz. Clearly, the most unfavorable case is $m=1$, yielding the dc value of $\tilde{\Omega}^*_{v_i}=V_i/2\rho\omega$. Other values of m, which cause rectification are $m=2N+1$, $N=1,2,3,\ldots$ for which the last factor in Eq. (63) yields $\cos\pi(2N+1+2Nn)$, which is ±1 regardless of n. For noninteger values, the beat frequency is $\mu=\nu-\omega=(m-1)\omega$, and the period is $T'=T/(m-1)$.

The amplitude of the positional deviation $\tilde{R}_{v_i}$ due to $\tilde{\Omega}^*_{v_i}$ at the beat frequency μ is determined by substituting $j\mu$ into the Schuler pendulum transfer function $1/s(\omega_s^2+s^2)$ obtaining

$$|\tilde{R}_{v_i}(\mu)| = \tilde{\Omega}^*_{v_i} g\,\frac{1}{\mu(\omega_s^2-\mu^2)} \tag{65}$$

For $\mu\ll\omega_s$ $|\tilde{R}_{v_i}(\mu)|\cong\tilde{\Omega}^*_{v_i}R_E/\mu$, which indicates a large amplitude building up at the very low frequency μ, for $\mu\gg\omega_s$, however, $|\tilde{R}_{v_i}(\mu)|=\tilde{\Omega}^*_{v_i}g/\mu^3$ indicating a rapid decrease with μ, and at $\mu=\omega_s$ the amplitude builds up at the Schuler frequency ω_s.

It follows, therefore, that only for $\mu\to0$ and $\mu\approx\omega_s$ large errors in $\tilde{R}_{v_i}$ will slowly build up. The probability of μ retaining a small value for a substantial fraction of the Schuler period is very low. Moreover, it is possible to control ω so that it is always sufficiently shifted from ν.

VIII. Wide-Band Random Accelerometer Noise

Detailed data of a typical forced balance type accelerometer show an rms value $\sigma_{n_i}\cong20$ μg. The noise source is at the detector located at the input of the high-gain current feedback amplifier. Consequently, the power spectrum density at low frequencies is very low, rising to a peak at 60 Hz and dropping again at a slope of 12 dB/Oct, and in accordance with the frequency characteristic of the closed-loop compensation network. A detailed analysis, not shown here, incorporating this noise model, the sgn $(\cos\omega t)$, integration and sample and hold operations of the signal processor, shows that the power spectrum density at zero frequency at the processor output is $1.04\times10^{-3}\ \sigma^2_{n_i}$ $(\mu g)^2$s. The autocorrelation function is approximately triangular crossing zero close to $\tau=T$. Thus, at the processor output, the effective noise can be modeled as white noise. This level of noise contributes negligible positional divergence. The foregoing result can easily be interpreted as follows. The very low frequency components being originally small are almost cancelled by the sgn$(\cos\omega t)$ operation. The very high frequency components, again are largely averaged by the intergration over T. Thus, accelerometer noise has a small effect on the angular rate measurement.

IX. Nonlinearities of Accelerometers

A. Even Nonlinearity $f(x)=x+a_2x^2$

The accelerometer input a_i, e.g., for $i=x$ is

$$a_x = F_x + bq\cos\omega t + br\sin\omega t \tag{66}$$

where $b=2\omega\rho$. Substituting Eq. (66) into $f(x)$, and rearranging, the output a_{x0} is

$$a_{x0}=F_x+a_2F_x^2+(1+2a_2F_x)\,bq\cos\omega t + (1+2a_2F_x)\,br\sin\omega t+(a_2/2)\,b^2\,(q^2+r^2) + (a_2/2)\,b^2\cos2\omega t\,(q^2-r^2)+2a_2b^2qr\sin\omega t\cos\omega t \quad (67)$$

Multiplying by $\mathrm{sgn}(\cos\omega t)$ and integrating over T to obtain q, all but the second term vanish. The second term contributes the estimate $\hat{q}$

$$\hat{q}=q(1+2a_2F_x) \quad (68)$$

Since F_x is stationary and assumed to be zero mean, $\hat{q}$ is correct in the mean. The even nonlinearity therefore results in a random zero mean scale factor error of $\hat{q}$.

B. Odd Nonlinearity $f(x)=x+a_3x^3$

Proceeding as before, we obtain:

$$a_{x0}=F_x+a_3F_x^3+(1+3a_3F_x^2)\,bq\cos\omega t + (1+3a_3F_x^2)\,br\sin\omega t+3a_3F_xb^2\,(r^2+q^2) +3a_3F_xb^2q^2\cos2\omega t-3a_3F_xb^2r^2\cos2\omega t+3a_3b^3q^2r\sin\omega t +3a_3b^3qr^2\cos\omega t+a_3b^3r\sin^3\omega t\,(r^2-3q^2) +a^3b^3q\cos^3\omega t\,(q^2-3r^2)+3a_3F_xb^2rq\sin2\omega t$$

To obtain q, multiplying by $\mathrm{sgn}(\cos\omega t)$ and integrating over T, only the terms with $\cos\omega t$ are retained, thus

$$\hat{q}=q\,[1+3a_3\,(F_x^2+b^2r^2)\,] \quad (69)$$

Thus, an odd nonlinearity in the accelerometers introduces a nonzero mean scale factor error $3a_3\,(F_x^2+b^2r^2)$.

Conclusion

Nonlinearities of the accelerometer introduce scale factor errors in the measurement of Ω_i, the odd nonlinearity having the more significant effect. Typical values for a_2 are $20\mu g/g^2$, which indicates quite negligible error in Ω_i.

X. Realization of the Signal Separation Processor

A schematic diagram of the processor separating Ω_i and F_i from a_i is shown in Fig. 5. a_i $(i=x,y,z)$ is applied to the input amplifier A_1, which is provided with a gain switch S_R triggered by V_R, so as to reduce the gain by a factor of 10 in accordance with Sec. I. V_R is generated by a threshold circuit, which operated whenever $|a_i|$ exceed the maximum admissible input. The control signals that trigger the switches S_2 to S_9 are shown in Fig. 6.

These signals originate from a free running multivibrator generating the pulses V_1 at the frequency $4f$, $f=1/T$. By means of a J-K flip-flop, the symmetric square wave V_2 at frequency $2f$ is generated. From it, by two additional J-K flip-flops, the signals V_3 and V_3' at frequency f are generated from the positive and negative steps of V_2. V_3' triggers another monostable multivibrator, which generates V_4 and $\bar{V}_4$. $\bar{V}_4$ triggers an additional J-K flip-flop, which generates V_5 and $\bar{V}_5$.

V_3 controls S_1, so that with A_5 $u_2=u_1\,\mathrm{sgn}(\cos\omega t)$. A_2 and A_2' are identical integrators which, with u_1 at their inputs, perform the integration $\int_0^T a_i(t)\,dt$. $S_2,S_2';S_3,S_3';S_4,S_4'$ are controlled by $V_5,\bar{V}_5$. These switching operations cause A_2 and A_2' to operate alternatively so that each integrator has a complete period T to permit a perfect reset after the preceding integration. A similar switching scheme with S_5,S_5'; S_6,S_6'; S_7,S_7' operates with integrators A_6,A_6' which, with u_2 at their inputs, perform the integration $\int_0^T a_i\mathrm{sgn}(\cos\omega t)\,dt$. The sample and hold circuits by means of $A_3,A_4;A_7,A_8$ are of standard design, and are controlled by the switches S_8,S_8'; S_9,S_9', respectively, which are triggered by $V_4,\bar{V}_4$. The pulse sequences $V_4,\bar{V}_4;V_5,\bar{V}_5$ are such that immediately after the sampling pulse $V_4,\bar{V}_4$ the corresponding integrator is reset, and the next sampling pulse operates on the alternative integrator. u_5,u_6 are consequently proportional to $\hat{F}_i^*$ and $\hat{\Omega}_i^*$, respectively.

XI. Performance Considerations and Experimental Results

In order to test the concept, an experimental signal separation processor, as described in Fig. 5, has been constructed with μA 725 and CA 3140 amplifiers, and CD 4066 switches. No special care has yet been given to the selection of resistors and capacitors. The amplifiers have voltage drift coefficients of about 1 $\mu V/°C$ and input leakage currents of about 50 nA. Without special provisions of temperature control, the total null point stability at room temperature was about 20 μV. For a maximum output of 6 V at u_5,u_6, and for a maximum angular rate $\Omega_i=200$ deg/s, this corresponds to an angular drift rate of $\sim$0.2 deg/h. This already is in the medium class IMU quality. The processor was tested for linearity in the F_i and Ω_i channels. F_i was simulated by a

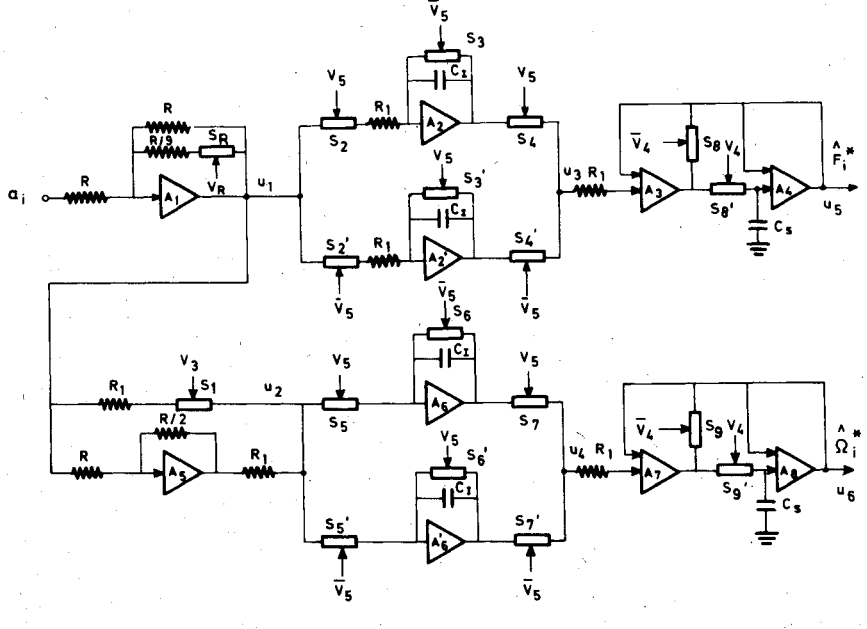

Fig. 5 Schematic diagram of signal processor for separation of F_i and Ω_i.

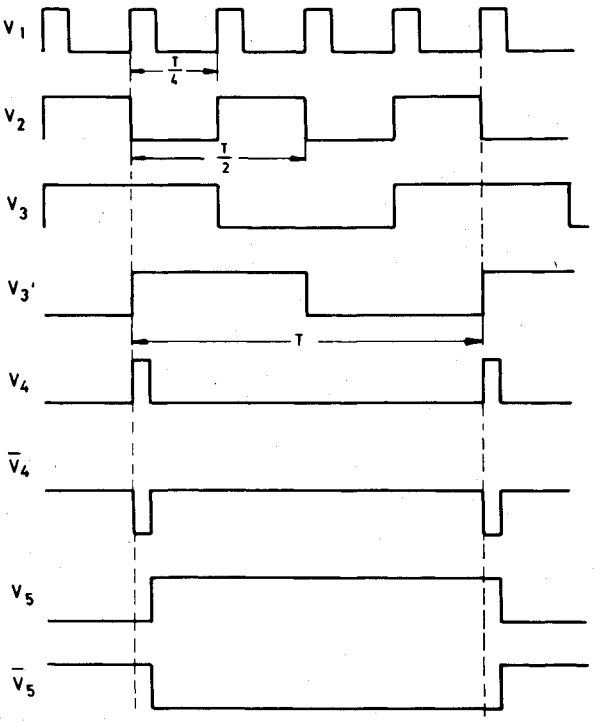

Fig. 6 Control and switching signals of the processor.

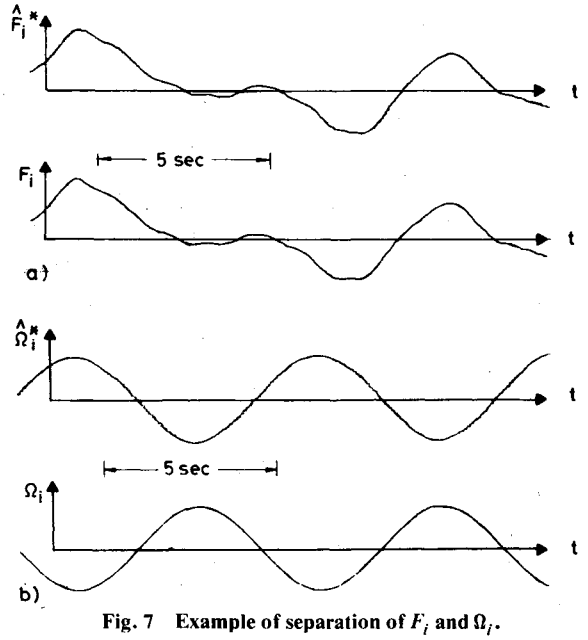

Fig. 7 Example of separation of F_i and Ω_i.

variable dc voltage, and Ω_i by a square wave proportional to V_3. The nonlinearities in $\hat{F}_i/F_i$ and $\hat{\Omega}_i/\Omega_i$ were better than 10^{-4}, and the "crosstalk" in $\hat{F}_i/\Omega_i$ and $\hat{\Omega}_i/F_i$ was 15-30 $\mu V/V$. For $\hat{\Omega}_i/F_i$ this is equivalent to about 1 deg/h at a typical bandwidth due to turbulence of $a \cong 1$ rad/s, which results in a positional error of ~1 n.mi/hr.

With newly available CMOS amplifiers, e.g., Intersil ICL 7650, leakage currents are in the order of 10 pA, and voltage drift coefficients are in the order of 0.01 μV/°C. With these performance data, which are two orders of magnitude better than in the present experimental model, the limiting factor, at present, is the variation of the leakage current in the integrator switches. This variation is in the order of 50 pA, and with typical values of the integrator capacitors the equivalent null point uncertainty at u_5, u_6 is expected to be about 0.5 μV. This is almost two orders of magnitude better than the 20 μV uncertainty of the experimental processor. Consequently, the angular drift rate Ω_{id} is expected to be in the order of 0.01 deg/h even without special provisions for temperature stabilization.

If the cross-product terms in Eq. (10) are compensated as shown in Fig. 2, the offset voltages of the multipliers should be considered. Typical values for multiplier offsets are 50 μV. Since their outputs are divided by $2\omega = 400$, the resulting error is 50/400 μV = 125 nV, which is negligible.

The signal separation processor was also tested with dynamic inputs of F_i and Ω_i for the purpose of performance demonstration. The input a_i was represented by the simultaneous signal of 2 V random first order Markov process with a bandwidth $a = 1$ rad/s representing F_i and a 2 V sine wave at frequency $\omega_i = 1$ rad/s, representing a frequency modulated angular rate. $\Omega_i(t) = \Omega_{imax} \sin \omega_i t$ was modulated by V_3 and added to F_i to form a_i. The results are shown in Fig. 7 indicating the performance of the processor. F_i and Ω_i are shown before their addition, and before the modulation of Ω_i by V_3 in order to enable a clear comparison with $\hat{F}_i^*$ and $\hat{\Omega}_i^*$. The recordings show the staircase trace in $\hat{\Omega}_i^*$ and $\hat{F}_i^*$ due the sample and hold operation. They indicate the linearity and the effective signal separation and practically the absence of crosstalk between the F_i and Ω_i channels.

XII. Conclusions

The analysis presented in this paper shows that a complete low-cost inertial measurement unit can be realized with a triad of rotating or vibrating accelerometers. The various dynamical and disturbance errors are rendered negligible by virtue of the method of signal separation described. The key feature of the concept is that it provides an essentially drift-free angular rate measurement along with the specific force measurements. With recent advances in CMOS technology, this drift-free property is hardly affected by the electronic processor. This property implies another potential savings since temperature control becomes, in most applications, unnecessary. Since the accelerometer measures both F_i and Ω_i, the maximum values for F_i for given maximum values of Ω_i may be more limited than in conventional inertial measurement units. However, in view of the large variety of potential applications with moderate-g missions, this possible limitation is more than balanced by the prospective substantial saving in cost.

The analysis described in this paper refers to a mechanization of rotating accelerometers. An alternative mechanization is by vibrating the accelerometers, which is mechanically simpler and does not have the large errors $\tilde{\Omega}_i^o$ due to orthogonal terms.

References

[1] Krishnan, V., "Measurement of Angular Velocity and Linear Acceleration Using Linear Accelerometers," *Journal of Franklin Institute,* Vol. 280, No. 4, Oct. 1965, pp. 305-315.

[2] Monaco, S.R. and Andly, D.R., "Schuler Tuned Vertical Indicating System," *Journal of Guidance and Control,* Vol. 1, Nov.-Dec. 1978, pp. 413-419.

[3] Killpatrick, J., "The Laser Gyro," *IEEE Spectrum,* Oct. 1967.

[4] Hector, F., "The Ramp Inertial Navigation System," *Philips Technical Review,* Vol. 29, Nos. 3-4, 1968, pp. 69-85.

[5] Merhav, S.J., "Low Cost Autonomous Navigation Method for Moderate-g Missions," *Journal of Guidance and Control,* Vol. 3, No. 5, Sept.-Oct. 1980, pp. 405-415.

[6] Garg, S.C., Morrow, L.D., and Mamek, R., "Strapdown Navigation Tehnology: A Literature Survey," *Journal of Guidance and Control,* Vol. 1, May-June 1978, pp. 161-172.

[7] Craig, R.J.G., "Theory of Operation of an Elastically Supported Tuned Gyroscope," *IEEE Transactions on Aerospace and Electronic Systems,* Vol. AES-8, No. 3, May 1972, pp. 280-288.

[8] "Q-Flex Servo Accelerometers," Sundstrand Data Control, Publication No. 2123/578, 1978.

[9] Schuler, A.R., et al., "Measuring Rotational Motion with Linear Accelerometers," *IEEE Transactions on Aerospace and Electronic Systems,* May 1967, pp. 465-471.

[10] "ICL 7650 Chopper Stabilized Amplifier," Intersil Publication No. 8-80-00A, 1980.

[11] "GG 2500 Magnetohydrodynamic Two-Axis Rate Sensor," Honeywell Publication No. 4085, 1976.